https://dx.doi.org/10.21577/0103-5053.20200191

J. Braz. Chem. Soc., Vol. 31, No. 11, 2430-2438, 2020
Printed in Brazil - ©2020 Sociedade Brasileira de Química

Article

Blue-Emitting MWO_4:Tm^{3+} (M: Sr, Ba) Phosphors Prepared by Coprecipitation Method at Room Temperature

Edson L. Gaiollo,[a] Renan P. Moreira,[a] Maria C. F. C. Felinto,[a] Helliomar P. Barbosa,[b] Cássio C. S. Pedroso,[b] Ercules E. S. Teotonio,[c] Oscar L. Malta[c,d] and Hermi F. Brito*[,b]

[a]*Instituto de Pesquisas Energéticas Nucleares (IPEN-CQMA), Av. Prof Lineu Prestes, 2242, 05508-000 São Paulo-SP, Brazil*

[b]*Departamento de Química Fundamental, Instituto de Química, Universidade de São Paulo, Av. Prof Lineu Prestes, 748, 05508-900 São Paulo-SP, Brazil*

[c]*Departamento de Química, Universidade Federal da Paraíba, 58051-970 João Pessoa-PB, Brazil*

[d]*Departamento de Química Fundamental, Universidade Federal de Pernambuco, 50670-901 Recife-PE, Brazil*

MWO_4 host matrices (M: Sr, Ba) doped with different Tm^{3+} concentrations (0.02, 0.04, 0.06, 0.08 and 0.10 mol%) have been successfully prepared by the coprecipitation method at room temperature. The as-prepared nanophosphors were characterized by infrared spectroscopy showing intense absorption bands in the range of 700-1000 cm^{-1} attributed to the symmetrical and asymmetrical stretching vibrations (ν) of the tetrahedral $[WO_4]^{2-}$ group. The X-ray diffraction (XRD) measurements reveal the tetragonal scheelite phase with the $I4_{1/a}$ (No. 88) space group. The emission spectra of the MWO_4:Tm^{3+} materials are dominated by the highest intensity narrow band of the intraconfigurational $^1D_2 \rightarrow {}^3F_4$ transitions in the blue region (ca. 456 nm) arising from the Tm^{3+} ions. Additional low-intensity emission bands originated from the $^1G_4 \rightarrow {}^3H_6$ (ca. 475 nm), $^1G_4 \rightarrow {}^3F_4$ (660 nm) and $^3H_4 \rightarrow {}^3H_6$ (700 nm) transitions are also observed. These optical results indicate that the materials can be used as an alternative to blue-emitting markers.

Keywords: blue-emitting, thulium, strontium and barium tungstates, coprecipitation method, photoluminescence

Introduction

In the last decades, inorganic host lattices doped with trivalent rare-earth ions (RE^{3+}) have been extensively studied due to the remarkable optical properties resulting from their 4f-4f transitions. The positions of the absorption and emission bands are practically independent of the ligand field around the RE^{3+} ion due to the effective shielding of the 4f-subshell by the external $5s^2$ and $5p^6$ subshells. These spectroscopic features lead to atomic-like transitions, showing sharp lines with high emission color purity.[1,2]

Nano- and micro-structured photonic materials with homogeneous morphology that present excellent monodispersity in bulk scale play important roles in the areas of electronic, optical, magnetic, catalytic, and chemical phenomena.[3-7] In particular, the trivalent rare-earth ions doped tungstates $[WO_4]^{2-}$ have been extensively studied during the past decades, mainly owing to their very interesting photoluminescent properties.[1]

Since the $CaWO_4$ matrix presents excellent chemical, thermal and luminescence properties, it has been extensively used in solid-state lasers, displays, scintillating materials, fiber-optical communication, etc.[8-11] For example, $CaWO_4$ matrix shows an intense broad emission band in the spectral range of 300-600 nm with a maximum at around 420 nm, exhibiting a blue-emission color assigned to the $O^{2-}(2p) \rightarrow W^{6+}$ ligand-to-metal charge transfer (LMCT) transitions from the $[WO_4]^{2-}$ groups under UV excitation.[10,12,13] However, the excitation energy of the doped MWO_4:RE^{3+} (M: Mg, Ca, Sr or Ba) may be efficiently transferred to RE^{3+} ions.[10,12,13]

In the last years, photoluminescence materials containing the MWO_4:RE^{3+} (M: Mg, Ca, Sr or Ba)

*e-mail: hefbrito@iq.usp.br
Dedicated to Prof Henrique Eisi Toma on the occasion of his 70th birthday.

matrices doped with Eu^{3+} and Tb^{3+} ions, which shows red and green emission colors, have been intensively reported.[13,14] On the other hand, the luminescence study arising from blue-emitting materials based on the Tm^{3+} ion doped into the tungstate host lattice is barely reported in the literature.

Tm^{3+} ions give rise to blue emission color from the $^1D_2 \rightarrow {}^3F_4$ transition in several host inorganic matrices.[15] The thulium ion can act as an activator in the development of the new luminescent materials for different applications in luminescent display devices, in plasma display panels (PDPs), for anti-counterfeiting, and in biological systems.[16-19]

In the last few decades, a large number of luminescent materials acting as blue emitters have been developed.[20-29] For example, efficient bright blue luminophores using the different activator ions Ce^{3+} ($Ba_9Al_2Si_6O_{24}$:Ce^{3+})[24] and Eu^{2+} ($Sr_2MgSi_2O_7$:Eu^{2+}, Dy^{3+})[30] present broad emission bands originated from the $4f^05d^1 \rightarrow 4f^1$ and $4f^65d^1 \rightarrow 4f^7$ interconfigurational transitions, respectively. On the other hand, the Tm^{3+} ion exhibits narrow blue emission lines assigned to the 4f-4f intraconfigurational transitions, showing monochromatic character.

In addition, trivalent thulium ions are known to offer many features in this spectral region due to the intraconfigurational $4f^{12}$ transitions with total degeneracy of only 91 crystal field levels. Furthermore, the electronic transitions between the ground ($^3H_6$) and excited ($^3H_{4-5}$, $^3F_{2-4}$, $^3P_{0-2}$, $^1D_2$, $^1G_4$, $^1I_6$, and $^1S_0$) states occur in the spectral range from 5,000 to 40,000 cm^{-1}, except for the $^1S_0$ level at 74,000 cm^{-1}. The $^3F_4 \rightarrow {}^3H_6$ and $^3H_4 \rightarrow {}^3F_4$ transitions are of great interest in surgery, optical communications, and remote sensing.[31] Towards the achievement of compact ultraviolet-blue lasers, the Tm^{3+} doped host is one of the most studied systems due to its radiative emissions at 360, 455 and 475 nm assigned to the $^1D_2 \rightarrow {}^3H_6$, $^1D_2 \rightarrow {}^3F_4$, and $^1G_4 \rightarrow {}^3H_6$ transitions, respectively.[32-35] Usually, Tm^{3+} materials show only weak 4f-4f emission because of the small energy gap between their emitting and lower energy levels; this increases the probability of nonradiative transitions.

In this work, we report the synthesis of luminescent MWO_4:Tm^{3+} (M: Ba, Sr) nanomaterials prepared by the coprecipitation route and their photonic properties. The $[WO_4]^{2-}$ LMCT states of the host matrix are also discussed. Furthermore, the 4f-4f electronic transitions originated from Tm^{3+} ion doped into the tungstate matrix are analyzed. The photoluminescence features arising from the trivalent thulium ion indicate that the materials can be used as efficient blue-emitting phosphors.

Experimental

Synthesis

The MWO_4:Tm^{3+} (M: Sr, Ba) materials were prepared by using an aqueous solution of Na_2WO_4 and $M(NO_3)_2$ (99.99% Sigma-Aldrich, São Paulo, Brazil). Stoichiometric quantities of $M(NO_3)_2 \cdot xH_2O$ and $Na_2WO_4 \cdot 2H_2O$ precursors were dissolved separately in deionized water.[13] The $Tm(NO_3)_3$ aqueous solution with concentrations of 0.02, 0.04, 0.06, 0.08, and 0.10 mol% was added into the $M(NO_3)_2$ aqueous solution. After that, the Tm^{3+} and M^{2+} resulting solution was added dropwise into the $[WO_4]^{2-}$ solution and stirred at room temperature (ca. 300 K) for 3 h. Finally, the white crystalline powders were filtered, dried, and stored under reduced pressure in a vacuum desiccator.

The infrared absorption spectra were measured using KBr pellets on a Bomem MB100 FTIR in the spectral region from 400 to 4,000 cm^{-1}. X-ray powder diffraction (XPD) patterns of the samples were registered with a Rigaku Miniflex II using Cu $K\alpha_1$ (1.5406 Å) radiation at 30 kV and 15 mA in 2θ interval of 10-80° with step size 0.02° and step measuring time of 1 s. The average crystallite sizes were estimated from the diffraction data by using the Scherrer formulae (equation 1),[36] where ϕ_{hkl} is the average grain size, λ is the X-ray wavelength, θ is half of the Bragg angle, and β is the full width at half maximum (FWHM) of the selected reflection. In this work, the (1 1 2) reflection (2θ: 28°) was used in the calculations. To correct the broadening due to the diffractometer setup from the β_s, it was used $\beta^2 = \beta_s^2 - \beta_r^2$, where β_s and β_r are the FWHM of the material and reference (NaCl: 0.149; 31.7°; *hkl*: 2 0 0), respectively.

$$\phi_{hkl} = \frac{0.9\lambda}{\beta \cos\theta} \quad (1)$$

The scanning electron microscopy (SEM) images of as-prepared MWO_4:Tm^{3+} (M: Sr, Ba) materials dispersed with chloroform were obtained by direct deposition on a carbon sample holder. A SEM JEOL Neoscope JCM-5000 Cannon equipment with a conventional tungsten filament, acceleration voltages 5-15 kV and maximum magnification capacity of ×40,000 for observation in low and high vacuum (30 Pa) were employed. Photoluminescence data of the materials containing Tm^{3+} ion were recorded at room and liquid nitrogen temperatures (77 K) by using a Fluorolog-3 spectrofluorometer (Horiba) presenting excitation and emission double-grating monochromators of 0.22 m. The 450 W pulsed Xe lamps were used as an excitation source. Luminescence decay curves were obtained by

using a 150 W pulsed lamp and recorded in a SPEX 1934D phosphorimeter.

Results and Discussion

Characterization

The undoped and doped MWO_4 host matrices (M: Ba^{2+}, Sr^{2+}) with different Tm^{3+} concentrations (0.02, 0.04, 0.06, 0.08 and 0.10 mol%) were synthesized by the coprecipitation method at room temperature, without subsequent calcination. This is a fast, economical and straightforward synthesis method to obtain luminescent nanomaterials, which does not require energy consumption and is an environmentally friendly method.[14]

The X-ray powder diffraction (XPD) patterns of all samples are ascribed to scheelite structure with the space group $I4_{1/a}$ (Powder Diffraction File (PDF) entries: No. 8-0490; No. 43-0646) data for the tetragonal phase (Figures 1a and 1b). No additional diffraction peaks in the XPD patterns originating from $Tm_2(WO_4)_3$ or any other phase were observed, which indicates that the as-prepared materials are a unique phase, indicating an efficient synthesis of the MWO_4:Tm^{3+} phosphors. These XPD data also confirm the successful incorporation of the Tm^{3+} ion in the host lattice. It is noteworthy that the ionic radius of Ba^{2+} and Sr^{2+} (1.42 and 1.26 Å, respectively) are larger than the ionic radius of the Tm^{3+} (1.13 Å) which is not totally in agreement with Vegard's law. However, the X-ray diffractograms show no segregation phase for these materials with coordination number 8 (Figure 1c).[37] Due to the small difference between the ionic radii, it is possible that the Tm^{3+} ion substitutes the M^{2+} site in the crystalline lattice.

The crystallite sizes and interplanar distances of $SrWO_4$ and $BaWO_4$ matrices doped with 0.02 to 0.10 mol% Tm^{3+}

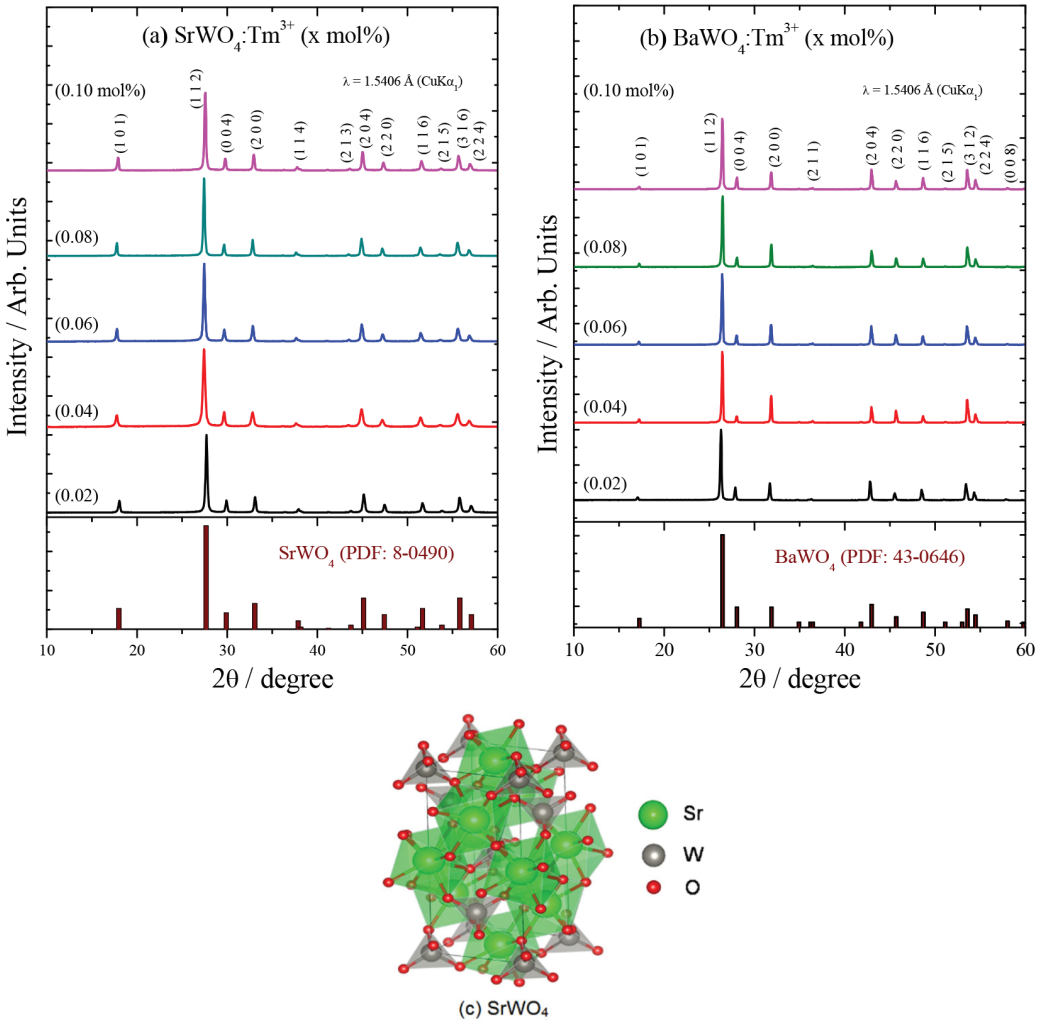

Figure 1. XPD patterns of undoped and doped (a) $SrWO_4$:Tm^{3+} and (b) $BaWO_4$:Tm^{3+} materials (0.02, 0.04, 0.06, 0.08 and 0.10 mol%). Vertical bars indicate the standard PDF (No. 8-0490; No. 43-0646) data for the tetragonal phase; (c) a schematic VESTA[38] representation of the tetragonal structure of the $SrWO_4$ showing the tetrahedral [WO_4] and tetragonal antiprism [SrO_8] units. Structural data adapted from reference 36.

ion are listed in Table S1 (Supplementary Information (SI) section). It is expected that the expansion of the ionic radii of the alkaline-earth ions ($r_{Sr^{2+}} < r_{Ba^{2+}}$) would cause an increase of the crystallite sizes. The ionic radii difference between Tm^{3+} and M^{2+} (Sr^{2+} and Ba^{2+}) can promote crystalline lattice distortion around the luminescent thulium activator.[37]

The diffraction peaks in Figure 1 shift to lower angles from $SrWO_4$:Tm^{3+} to $BaWO_4$:Tm^{3+} due to the fact that the radius of Sr^{2+} ions (1.26 Å) is smaller than that of the Ba^{2+} ions (1.42 Å). In this case, $BaWO_4$ has the biggest radii leading to a larger crystal plane spacing d in accordance with the Bragg's equation $2d\sin\theta = n\lambda$ (λ is the wavelength of X-ray, θ is the angle, and n is a positive integer). The d values of (1 1 2) were calculated and the results are listed in Table S1 (SI section).

The Fourier transform infrared (FTIR) absorption spectra of the as-synthesized samples $BaWO_4$:Tm^{3+} and $SrWO_4$:Tm^{3+} phosphors are shown in Figure 2. The absorption bands at 3454 and 1630 cm^{-1} are assigned to O–H stretching vibration and H–O–H bending vibration,[39,40] respectively, which are characteristic vibrations of water molecules physically adsorbed on the sample surface and the materials and the KBr pellets. A strong absorption band around 820 cm^{-1} is related to O–W–O stretches in the MWO_4-type scheelite oxides. The tetrahedral $[WO_4]^{2-}$ groups have S_4 site symmetry and show main absorption bands in the spectral region from 500 to 1000 cm^{-1}. The bands centered around 928 and 825 cm^{-1} correspond to the $\nu 1$ and $\nu 3$ modes of the $[WO_4]^{2-}$ groups, respectively.[41] The narrow absorption bands at 400 cm^{-1} and below, assigned to the δ(M–O) bending modes for the materials containing Ba and Sr,[42] are out of our experimental range. The non-doped and doped MWO_4 systems show very similar FTIR behavior, and the absorption bands assigned to Tm–O stretching are not observed owing to low Tm^{3+} concentrations.

The scanning electron microscopy (SEM) images show that the non-doped $BaWO_4$ and $SrWO_4$ matrices present crystallites with rice-grain shapes (Figures 3a and 3d). When the $BaWO_4$ matrix is doped with Tm^{3+} ion with a concentration of 0.02 mol%, it shows a bipyramidal shape (Figures 3b and 3e). On the other hand, $SrWO_4$:Tm^{3+} materials doped at the highest concentration (0.1 mol%) exhibit monodispersed micro-agglomerates, differently from the observed for $BaWO_4$:Tm^{3+} (Figures 3c and 3f).

Photoluminescence investigation

MWO_4:Tm^{3+} blue-emitting phosphors

The excitation and emission spectra of the MWO_4 matrices doped with Gd^{3+} (1.0 mol%) ion were also recorded to investigate energy levels from the tungstate matrices (Figure 4). It is known that the Gd^{3+} ion presents a large energy gap (ca. 32000 cm^{-1}) between the $^8S_{7/2}$ ground state and the first $^6P_{7/2}$ excited state to obtain information on LMCT states from $[WO_4]^{2-}$ group. The excitation of the $SrWO_4$ and $BaWO_4$ matrices show two broad absorption bands centered at 270 and 375 nm assigned to the LMCT states from $[WO_4]^{2-}$ group (Figure 4a). Besides, the emission spectra of the $SrWO_4$:(0.1 mol%) Gd^{3+} and $BaWO_4$:(0.1 mol%)Gd^{3+} samples present two broad emission bands at 425 and 480 nm characteristic to the LMCT states from $[WO_4]^{2-}$ group (Figure 4b).

The excitation spectra of the MWO_4:Tm^{3+} phosphors (M: Sr, Ba) were recorded at room temperature in the range from 250 to 375 nm (Figure 5), monitoring the emission in the $^1D_2 \rightarrow {}^3F_4$ transition (456 nm). They consist of

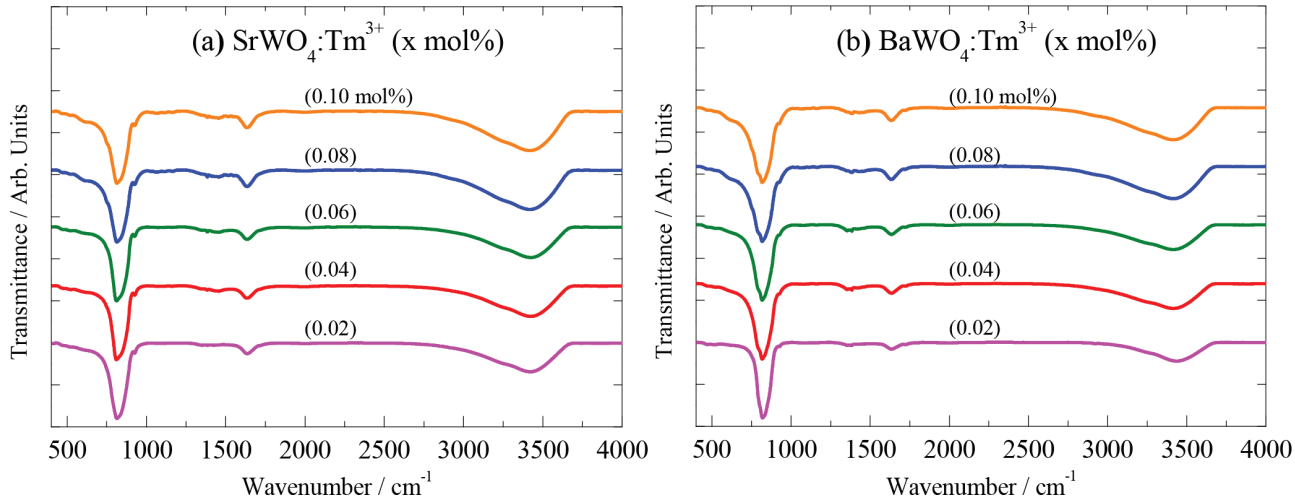

Figure 2. FTIR absorption spectra (KBr) of (a) $SrWO_4$:Tm^{3+} and (b) $BaWO_4$:Tm^{3+} (0.02, 0.04, 0.06, 0.08 and 0.10 mol%) materials obtained by coprecipitation method.

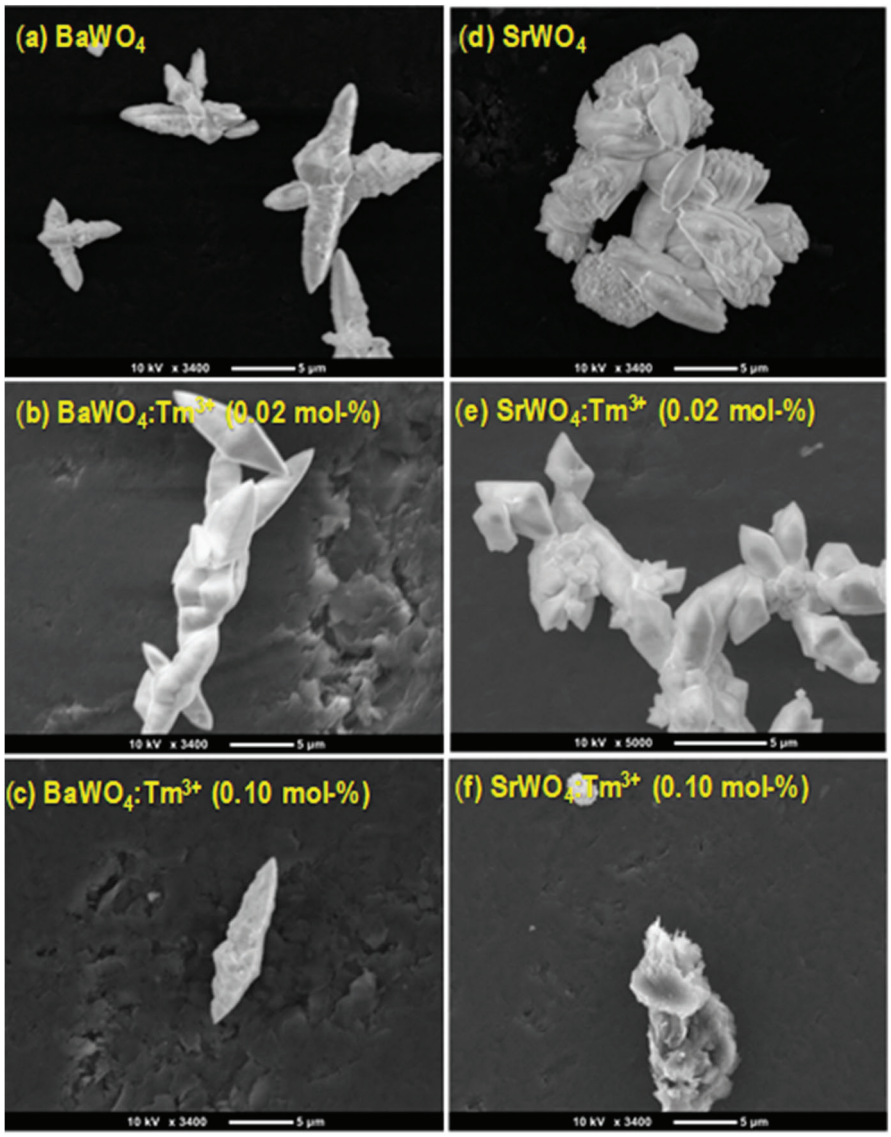

Figure 3. SEM images of micro agglomeration of crystals of non-doped and doped $SrWO_4$ and $BaWO_4$ (with 0.02 and 0.1 mol% Tm^{3+}) obtained by coprecipitation method.

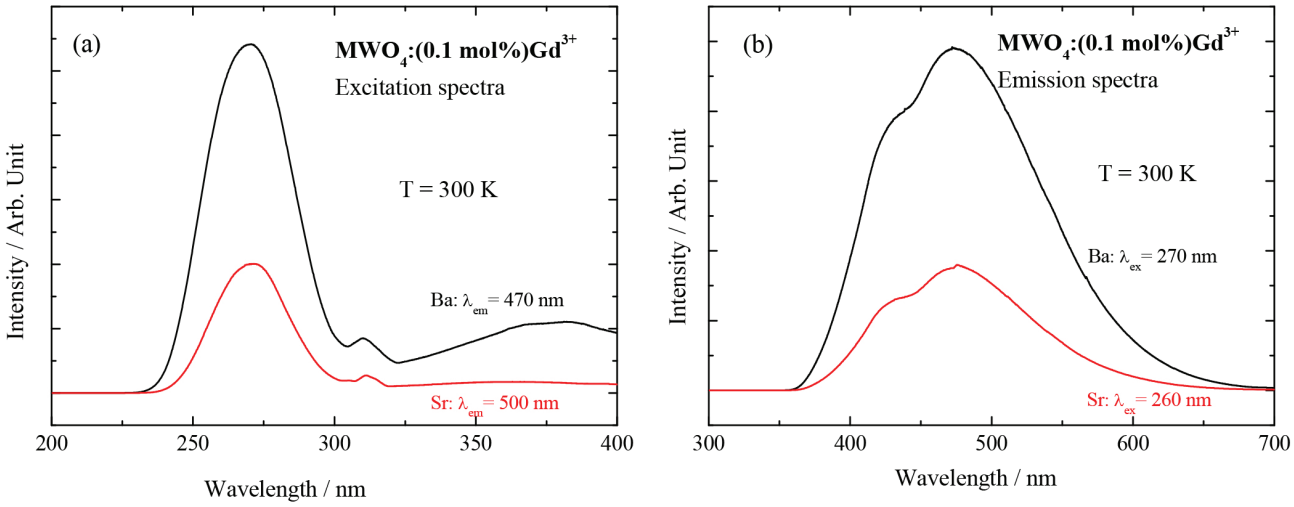

Figure 4. (a) Excitation and (b) emission spectra of the $SrWO_4$:(0.1 mol%)Gd^{3+} and $BaWO_4$:(0.1 mol%)Gd^{3+} compounds recorded at room temperature (300 K).

broad absorption bands with a maximum at about 255 and 280 nm assigned to the $O^{2-}(2p) \rightarrow W^{6+}$ LMCT transition MWO_4 for Sr^{2+} and Ba^{2+}, respectively.[12,43-46] In the longer wavelengths region, the 4f-4f transitions within the Tm^{3+} $4f^{12}$ configuration can be detected with the highest absorption intensity compared to excitation in the LMCT states, which is assigned to transition from the $^3H_6$ ground state to the $^1D_2$ excited state of Tm^{3+} centered at 360 nm (Figure 5).

The highest blue emission band centered at 456 nm is observed for all MWO_4:Tm^{3+} materials as shown in Figures 6a and 6b, except for the thulium concentration at 0.02 mol%. It corresponds to the emission from $^1D_2$ excited state to the $^3F_4$ state from Tm^{3+} ion. In addition, the low emission intensity bands from thulium are also present at ca. 660 nm assigned to the $^1G_4 \rightarrow {}^3F_4$ transition, while the $^1G_4 \rightarrow {}^3H_6$ transition is located at ca. 475 nm in the MWO_4:Tm^{3+} phosphors at 77 K. Besides, the highest emission intensity of Tm^{3+} in MWO_4 phosphors is $^1D_2 \rightarrow {}^3F_4$ transition located at the blue region, exhibiting high color purity, indicating that the MWO_4:Tm^{3+}

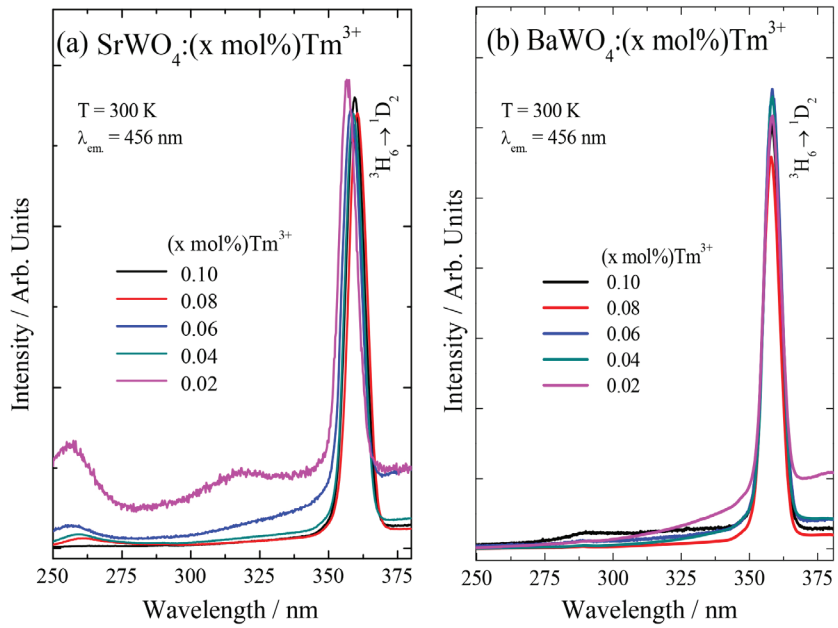

Figure 5. Excitation spectra of (a) $SrWO_4$:Tm^{3+} and (b) $BaWO_4$:Tm^{3+} materials (0.02 to 0.1 mol%) compounds recorded at 77 K.

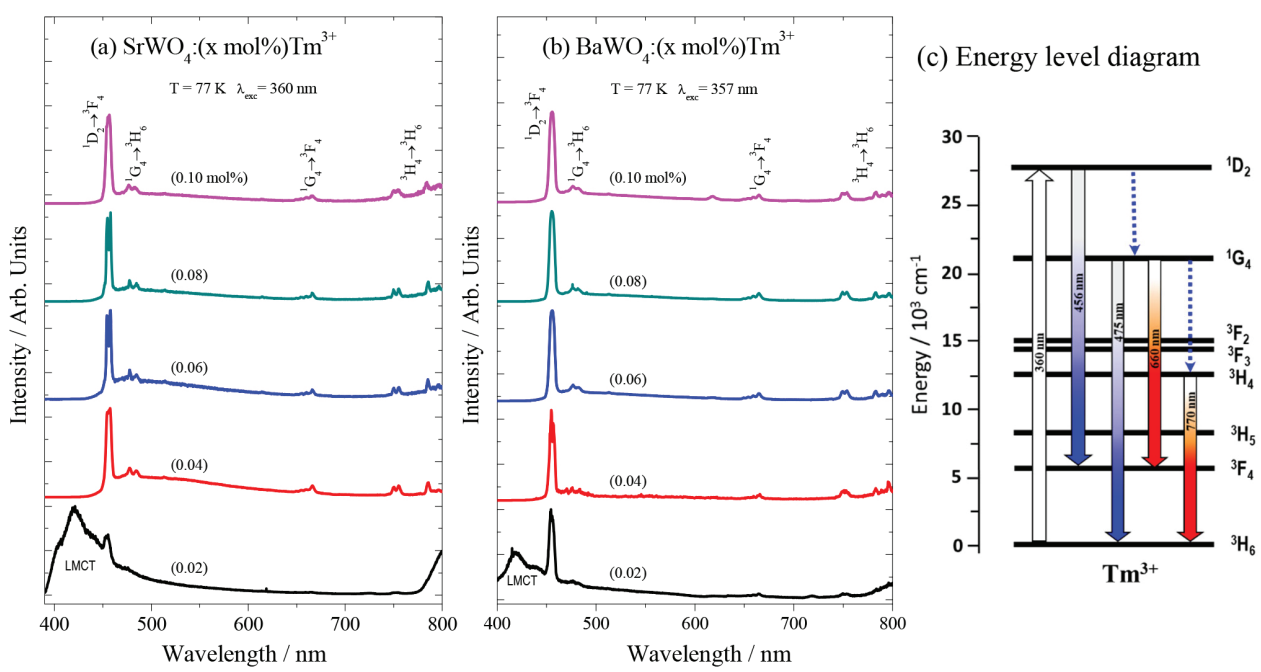

Figure 6. Emission spectra of (a) $SrWO_4$:Tm^{3+} and (b) $BaWO_4$:Tm^{3+} materials (0.02 to 0.1 mol%) recorded at 77 K; (c) partial energy level diagram.

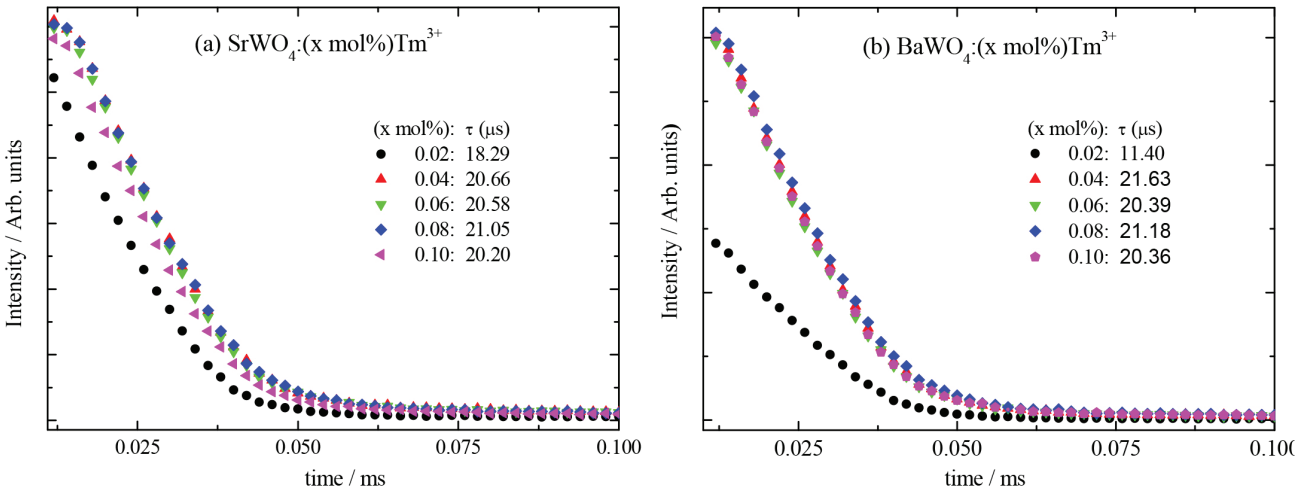

Figure 7. Luminescence decay curves of the $^1D_2$ emitting level of Tm^{3+} ions in the (a) $SrWO_4$:Tm^{3+} and (b) $BaWO_4$:Tm^{3+} materials (0.02 to 0.1 mol%) recorded at room temperature with λ_{em} ca. 456 nm and λ_{ex} ca. 360 nm. The emission intensities of all Tm^{3+} doped samples have been subtracted by the intrinsic emission by the host matrices.

materials can be used as blue-emitting markers. The partial energy level diagram (Figure 6c) shows the direct excitation at 360 nm assigned to the $^1D_2$ level of the Tm^{3+} ion. Besides, the narrow emission bands in the spectral regions 470, 660 and 770 nm are assigned to the $^1G_4 \rightarrow {}^3H_6$, $^1G_4 \rightarrow {}^3F_4$ and $^3H_4 \rightarrow {}^3H_6$ transitions, respectively (Figures 6a and 6b).

The luminescence lifetimes of the $^1D_2$ emitting level of Tm^{3+} were measured under excitation at around 360 nm, and the decay curves can be satisfactorily fitted with a single exponential. The short lifetime values are possibly due to surface defects or impurity ligands such as O–H in the samples that might act as channels of nonradiative decay (Figure 7). The average lifetimes for $^1D_2$ emitting level of Tm^{3+} ions of concentration from 0.02 to 0.1 mol% is ca. 20 μs for $SrWO_4$:$Tm^{3+}$and $BaWO_4$:Tm^{3+}.[47,48] In the case of the barium sample doped with 0.02 mol% concentration (Figure 7b) we have at the moment no explanation for the considerably different behavior with respect to the higher doping concentrations.

The chromaticity diagram (Figure 8) presents the coordinates of emission color for the MWO_4 host matrices (M: Ba, Sr) doped with different Tm^{3+} concentrations (0.02, 0.04, 0.06, 0.08 and 0.10 mol%).[49] Some materials emit in the blue region, close to the center of the chromaticity diagram, and some in the dark blue region, close to the vertices. The Commission Internationale de l'Éclairage (CIE) coordinates for $SrWO_4$:Tm^{3+} and $BaWO_4$:Tm^{3+} are reported in Table S2 (SI section) and agree with blue color. It is observed that the luminescent $SrWO_4$:Tm^{3+} and $BaWO_4$:Tm^{3+} materials doped with lowest thulium concentration (0.02 mol%) have high blue color contributions becoming an efficient and cheaper blue-emitting phosphor.

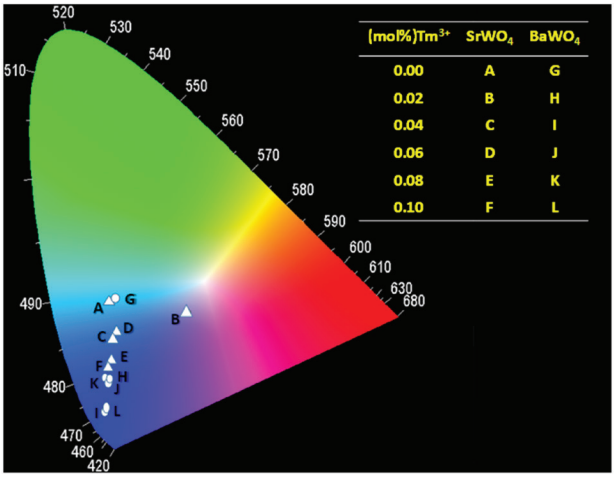

Figure 8. CIE chromaticity diagrams of the luminescent MWO_4:Tm^{3+} materials (M: Sr, Ba) presenting different thulium concentrations (0.02 to 0.1 mol%).

Conclusions

Doped MWO_4:Tm^{3+} (M: Sr, Ba) materials were successfully prepared through a classical coprecipitation method. This method offers many advantages in comparison to conventional procedures, such as simple operation, low cost, fast preparation and homogeneous morphology. Besides, it is performed at a lower temperature than the usual solid-state method, avoiding the formation of undesired phases induced by high temperatures. An eventual lowest component of the LMCT state, probably a triplet-type state, is deactivated non-radiatively extremely fast, and no energy transfer is operative. Under ultraviolet excitation at 355 nm assigned to the $^3H_6 \rightarrow {}^1D_2$ transition of the Tm^{3+}, the doped phosphors exhibit strong blue emission at 456 nm ($^1D_2 \rightarrow {}^3F_4$ transition). Moreover, the MWO_4:Tm^{3+} systems

are promising candidates suitable for applications as blue phosphors in optical markers and blue color lighting.

Supplementary Information

Supplementary information (crystallographic and luminescence data and CIE coordinates) are available free of charge at http://jbcs.sbq.org.br as PDF file.

Acknowledgments

Financial support is gratefully acknowledged from the Conselho Nacional de Desenvolvimento Científico e Tecnológico (CNPq) and the Coordenação de Aperfeiçoamento de Pessoal de Nível Superior (CAPES), the Fundação de Amparo à Pesquisa do Estado de São Paulo (FAPESP), and the Instituto Nacional de Ciência e Tecnologia-Nanotecnologia para Marcadores Integrados (INCT-INAMI).

Author Contributions

Edson L. Gaiollo was responsible for the experimental procedure, discussion, writing review and editing; Renan P. Moreira for the experimental procedure, discussion, writing review and editing; Maria C. F. C. Felinto for the experimental procedure, discussion, writing review and editing, conceptualization; Helliomar P. Barbosa for the discussion, writing review and editing, conceptualization; Cássio C. S. Pedroso for the discussion, writing review and editing, conceptualization; Ercules E. S. Teotonio for the discussion, writing review and editing, conceptualization; Oscar L. Malta for the discussion, writing review and editing, conceptualization; Hermi F. Brito (professor in chief) for the experimental procedure, discussion, writing review and editing, conceptualization.

References

1. Höppe, H. A.; *Angew. Chem., Int. Ed. Engl.* **2009**, *48*, 3572.
2. Keskar, M.; Gupta, S. K.; Phatak, R.; Kannan, S.; Natarajan, V.; *J. Photochem. Photobiol., A* **2015**, *311*, 59.
3. Kong, X. Y.; Ding, Y.; Yang, R.; Wang, Z. L.; *Science* **2004**, *303*, 1348.
4. Huang, S.; Zhang, X.; Wang, L.; Bai, L.; Xu, J.; Li, C.; Yang, P.; *Dalton Trans.* **2012**, *41*, 5634.
5. Wang, L.; Li, Y.; *Chem. Mater.* **2007**, *19*, 727.
6. Zhai, T.; Fang, X.; Bando, Y.; Dierre, B.; Liu, B.; Zeng, H.; Xu, X.; Huang, Y.; Yuan, X.; Sekiguchi, T.; Golberg, D.; *Adv. Funct. Mater.* **2009**, *19*, 2423.
7. Silver, J.; Martinez-Rubio, M. I.; Ireland, T. G.; Fern, G. R.; Withnall, R.; *J. Phys. Chem. B* **2001**, *105*, 948.
8. López, X.; Carbó, J. J.; Bo, C.; Poblet, J. M.; *Chem. Soc. Rev.* **2012**, *41*, 7537.
9. Kaczmarek, A. M.; Van Deun, R.; *Chem. Soc. Rev.* **2013**, *42*, 8835.
10. Miras, H. N.; Yan, J.; Long, D.-L.; Cronin, L.; *Chem. Soc. Rev.* **2012**, *41*, 7403.
11. Kaczmarek, A. M.; Liu, Y.-Y.; Van Der Voort, P.; Van Deun, R.; *Dalton Trans.* **2013**, *42*, 5471.
12. Kodaira, C. A.; Brito, H. F.; Felinto, M. C. F. C.; *J. Solid State Chem.* **2003**, *171*, 401.
13. Barbosa, H. P.; Kai, J.; Silva, I. G. N.; Rodrigues, L. C. V.; Felinto, M. C. F. C.; Hölsä, J.; Malta, O. L.; Brito, H. F.; *J. Lumin.* **2016**, *170*, 736.
14. Barbosa, H. P.; Silva, I. G. N.; Felinto, M. C. F. C.; Teotonio, E. E. S.; Malta, O. L.; Brito, H. F.; *J. Alloys Compd.* **2017**, *696*, 820.
15. Zhang, J.; Zhang, X.; Chen, C.; Shi, W.; Wang, X.; Han, B.; *J. Mater. Sci.: Mater. Electron.* **2018**, *29*, 6543.
16. Zhao, W.; An, S.; Fan, B.; Li, S.; *Appl. Phys. A: Mater. Sci. Process.* **2014**, *116*, 987.
17. Gieszczyk, W.; Marczewska, B.; Kłosowski, M.; Mrozik, A.; Bilski, P.; Sas-Bieniarz, A.; Goj, P.; Stoch, P.; *Materials* **2019**, *12*, 2861.
18. Xie, M.; Huang, Y.; Tao, Y.; Liang, H.; Su, Q.; *J. Electrochem. Soc.* **2010**, *157*, J401.
19. Shi, Y.; Yang, L.; Song, H.; Bai, Y.; Li, C.; Wang, Z.; *J. Mater. Sci.: Mater. Electron.* **2017**, *28*, 4192.
20. Zhang, Q.; Li, B.; Huang, S.; Nomura, H.; Tanaka, H.; Adachi, C.; *Nat. Photonics* **2014**, *8*, 326.
21. Wang, S.; *Coord. Chem. Rev.* **2001**, *215*, 79.
22. Zhu, D.; Zaffalon, M. L.; Pinchetti, V.; Brescia, R.; Moro, F.; Fasoli, M.; Fanciulli, M.; Tang, A.; Infante, I.; de Trizio, L.; Brovelli, S.; Manna, L.; *Chem. Mater.* **2020**, *32*, 5897.
23. Li, D.; Zhou, D.; Xu, W.; Chen, X.; Pan, G.; Zhou, X.; Ding, N.; Song, H.; *Adv. Funct. Mater.* **2018**, *28*, 1804429.
24. Teng, Y.; *Luminescence*, *in press*, DOI: 10.1002/bio.3915.
25. Zeng, H.; Duan, G.; Li, Y.; Yang, S.; Xu, X.; Cai, W.; *Adv. Funct. Mater.* **2010**, *20*, 561.
26. Sun, J.; Zhang, X.; Zhang, R.; *Mater. Lett.* **2020**, *267*, 127559.
27. He, H.; Sun, F.; Borjigin, T.; Zhao, N.; Zhu, G.; *Dalton Trans.* **2014**, *43*, 3716.
28. Kim, Y.; Yang, K.; Lee, S.; *J. Mater. Chem. C* **2020**, *8*, 7679.
29. Debnath, S.; Das, R.; *J. Mol. Struct.* **2020**, *1199*, 127044.
30. Lastusaari, M.; Jungner, H.; Kotlov, A.; Laamanen, T.; Rodrigues, L. C. V.; Brito, H. F.; Hölsä, J.; *Z. Naturforsch., B: J. Chem. Sci.* **2014**, *69*, 171.
31. de Camargo, A. S. S.; Andreeta, M. R. B.; Hernandes, A. C.; Nunes, L. A. O.; *Opt. Mater.* **2006**, *28*, 551.
32. Chung, J. H.; Ryu, J. H.; Lee, S. Y.; Kang, S. H.; Shim, K. B.; *Ceram. Int.* **2013**, *39*, 1951.

33. Dorosz, D.; Zmojda, J.; Kochanowicz, M.; Miluski, P.; Jelen, P.; Sitarz, M.; *Spectrochim. Acta, Part A* **2015**, *134*, 608.
34. Sinitsyn, V. V.; Redkin, B. S.; Kiselev, A. P.; Shmurak, S. Z.; Kolesnikov, N. N.; Kveder, V. V.; Ponyatovsky, E. G.; *Solid State Sci.* **2015**, *46*, 80.
35. Ryba-Romanowski, W.; Niedźwiedzki, T.; Komar, J.; Lisiecki, R.; Świrkowicz, M.; *J. Lumin.* **2015**, *162*, 134.
36. Klug, H. P.; Alexander, L. E.; *X-Ray Diffraction Procedures for Polycrystalline and Amorphous Materials*, vol. 4, 2nd ed.; John Wiley & Sons: New York, 1974.
37. Shannon, R. D.; *Acta Crystallogr., Sect. A* **1976**, *32*, 751.
38. Momma, K.; Izumi, F.; *J. Appl. Crystallogr.* **2008**, *41*, 653.
39. Nogueira, H. I. S.; Cavaleiro, A. M. V.; Rocha, J.; Trindade, T.; de Jesus, J. D. P.; *Mater. Res. Bull.* **2004**, *39*, 683.
40. Kato, A.; Oishi, S.; Shishido, T.; Yamazaki, M.; Iida, S.; *J. Phys. Chem. Solids* **2005**, *66*, 2079.
41. Porto, S. P. S.; Scott, J. F.; *Phys. Rev.* **1967**, *157*, 716.
42. Kodaira, C. A.; Brito, H. F.; Teotonio, E. E. S.; Felinto, M. C. F. C.; Malta, O. L.; Brito, G. E. S.; *J. Braz. Chem. Soc.* **2004**, *15*, 890.
43. Dieke, G. H.; Satten, R. A.; *Am. J. Phys.* **1970**, *38*, 399.
44. Holsa, J.; Lamminmaki, R.-J.; Antic-Fidancev, E.; Lemaitre-Blaise, M.; Porcher, P.; *J. Phys.: Condens. Matter* **1995**, *7*, 5127.
45. Liao, J.; Qiu, B.; Wen, H.; Chen, J.; You, W.; Liu, L.; *J. Alloys Compd.* **2009**, *487*, 758.
46. Ma, X.; You, Z.; Zhu, Z.; Li, J.; Wu, B.; Wang, Y.; Tu, C.; *J. Alloys Compd.* **2008**, *465*, 406.
47. Thongtem, T.; Phuruangrat, A.; Thongtem, S.; *Appl. Surf. Sci.* **2008**, *254*, 7581.
48. Murakami, S.; Herren, M.; Rau, D.; Morita, M.; *Inorg. Chim. Acta* **2000**, *300-302*, 1014.
49. Santa-Cruz, P. A.; Teles, F. S.; *Spectra Lux Software*, v.2.0 Beta; Ponto Quântico Nanodispositivos, RENAMI, UFPE, Recife, Brazil, 2003.

Submitted: May 6, 2020
Published online: September 18, 2020